EAN 2012
50th annual coference on experimental stress analysis

X-ray Diffraction Residual Stress (RS) Analysis as a Non–destructive Tool for Production Quality Control

Stanisław J.Skrzypek[1]

Abstract: Examples where analysis of residual stresses (RS) have important contribution in materials and processes characterization are described in the paper. In these works the *GID-*$sin^2\psi$ method based on the grazing incidence angle X-ray diffraction (called grazing incidence diffraction - GID) geometry and classical $sin^2\psi$ method are applied to macro-residual stresses measurement in surface layers after different kind of machining and surface preparation of machine parts made of various kind of materials like TiN, austenitic alloy, sinters and steels. Surface layers of different thickness can be investigated/measured by matching wavelength and incidence angle α of X-ray beam.

Keywords: grazing incidence x-ray diffraction, residual macroscopic stresses; non-destructive characterization; retained austenite; ball bearings, coatings

1. Introduction

Mechanical, thermal and thermo-mechanical treatments and various type of machining frequently used for surface finishing and strengthening effectively generate and/or release residual stresses (RS). These processes are activated by thermal stress field energy, diffusion processes, phase transitions, slip and dislocation climb and generation and/or annihilation of lattice defects. Heating and cooling during mechanical and/or thermal treatment cause temperature gradients, which are related to thermal stresses. For diffusionless transformations, thermal treatments may require high heating and/or cooling rates. Such heat treatments and additional surface machining are main factors in creating of RS. Annealing, slowly heating or cooling cause relaxation of RS. Cyclic mechanical loading also possibly contributes to relaxation of RS. Accompanying phase transformations, according to Le Chatelier 's principle, can be either enhanced or retarded by thermal stresses [1, 8].

2. Example of TiN coatings (Skrzypek, Baczmański 2000 and 2001) [1, 2, 7]

In the presented example *GID-*$sin^2\psi$ method was used where the $s_1(hkl)$ and $s_2(hkl)$ constants used for one $<a(\varphi,\psi)>_{(hkl)}$ vs. $sin^2\psi$ graph depend on the *hkl* reflection. Moreover, in the case of textured material, these constants depend on the orientation

[1] *AGH-University of Science & Technology, al. Mickiewicza 30, 30-059 Kraków, Poland*
skrzypek@uci.agh.edu.pl

distribution. Consequently these constants depend on the ψ *and* φ angles and $<a(\varphi,\psi)>_{(hkl)}$ vs. $sin^2\psi$ graph is not linear (Fig.1).

The *GID*-$sin^2\psi$ geometry and from five to eight diffraction lines (i.e.: {111}, {200}, {220}, {311}, {222}, {400} and {420}) were used for determination of the residual stresses in TiN coatings deposited on sintered WC carbide (sample no.V30, Tab.1) and on sintered high speed steel (sample no.T31, Fig.1). The coatings were produced by the CVD method in the case of V30 sample and by PVD for the other one. The Cu $K\alpha_1$ radiation was used with the Philips diffractometer (X-Pert MPD) and $CoK\alpha$ with the Bruker (D8 Advance) diffractometer. The diffraction patterns were recorded for two φ angles i.e. for 0 and 180 degrees.

The diffraction elastic constants (s_1 and s_2) were calculated from single crystal elastic constants (s_{1111} = 2.17 10^{-3} GPa^{-1}, s_{1122}= - 0.38 10^{-3} GPa^{-1}, s_{1212} = 1.49 10^{-3} GPa^{-1}) using the Voigt and Reuss approaches.

The macro-RS determined for different penetration depth are presented in the Table 1. The experimental lattice parameter $<a(\varphi,\psi)>_{(hkl)}$ (recalculated from measured $<d(\psi,\varphi)>_{(hkl)}$) is compared with the results of fitting for the Reuss and Voigt methods (Fig.1). For the Reuss method the crystal anisotropy is determined and the non-linear graph approaches the experimental values. The small texture of V30 sample had small influence on non-linearity of experimental points (Fig.1). The texture in this case is described by three weak fibers i.e. {773}<uvw>, {113}<uvw> and {013}<uvw>. The intensity of this texture is f(g)=1.6 [1, 2]. **There is no pronounced influence of the strong texture of T31 sample on values of measured RS, either. In this case one strong (f(g)=10) fiber appeared i.e. {111}<uwv> [2, 7].**

Tab.1. Residual biaxial stresses for assumption $\sigma^I_{11} = \sigma^I_{22}$ in TiN coatings deposited on WC carbide substrate. The *GID-sin*$^2\psi$ method was used and the penetration depth was calculated using G_x=0.95 and μ = 561 cm^{-1} for Cu $K\alpha_1$ [3]. The total thickness of the coating was 5 μm [2, 7].

Grazing angle (α) [deg]	Stress ($\sigma^I_{11}=\sigma^I_{22}$) [MPa] Reuss method	Stress ($\sigma^I_{11}=\sigma^I_{22}$) [MPa] Voigh method	Average stress ($\sigma^I_{11}=\sigma^I_{22}$) [MPa]	Penetration depth (t) [μm]
1	1582±37	1550±36	1566	0.9
3	1242±39	1194±38	1218	2.6
6	1107±43	1045±41	1076	4.8-5.2

Final remarks:

The correct diffraction elastic constants should be used for interpretation of the experimental data. These constants have to be calculated for different *hkl* reflections and various sample orientations. It is caused by crystal anisotropy which creates the nonlinearities on the strain vs. $sin^2\psi$ plot (Fig.1). These nonlinearities can be easily modelled using theoretical Reuss approach. The results provided here in Tab.1, which were obtained in two labs with two different diffractometers and wavelengths are closed each other [1, 2].

Although TiN coating on sample HSS steel represents quite strong texture the appropriate results for qusi-isotropic and anisotropic procedure of calculations differ a little.

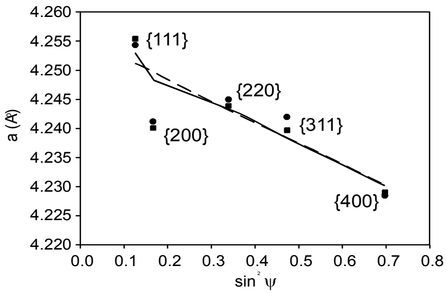

Fig.1. The example of $<a(\phi,\psi)>_{(hkl)}$ lattice parameters (elastic strain, refers to Tab.2, sample T31) are fitted to the experimental points for grazing incident angle $\alpha = 1°$ (t = 0.6 μm) . Calculated $<a(\phi,\psi)>_{(hkl))}$ values are connected using continues line for Reuss method and dashed line for Voigt method and compressive RS was establisced as (-) 3077 MPa [2, 7].

3. Baal bearings – samples, X-ray diffraction patterns and RS (Skrzypek at al 2007) [10]

Surfaces of super finished and also burnished of 100Cr6 steel ball bearings were examined by classical $sin^2\psi$ *and* GID-$sin^2\psi$ methods, taking special note of problems of real depth of X-ray penetration. Applying grazing angle geometry residual macro-stresses, retained austenite and additionally their surface layer properties versus depth i.e. gradients were evaluated. Theoretical calculations of residual macro-stresses due to transformed austenite and following measurnament were carried out for the ball bearings. Their mechanical burnishing caused phase transformation of austenite in the thin surface layer and large compressive residual stresses, about –700 MPa what was obligatory requirement by internal regulation of producer [10].

Samples were ball bearings made of 105Cr6 steel, which were prepared by different methods in order to obtain specific surfaces and surface layer properties. These were:

1. grinding and super finishing,
2. burnishing I, (2 hrs in rotating chamber with balls)
3. burnishing II, (3 hrs in rotating chamber with balls)

The mechanical burnishing consisted in balls striking each other during rotation of a cylindrical chamber during assumed time [10]. Results of quantitative phase analysis and RS measurnament are presented on figure 2 and in table 2.

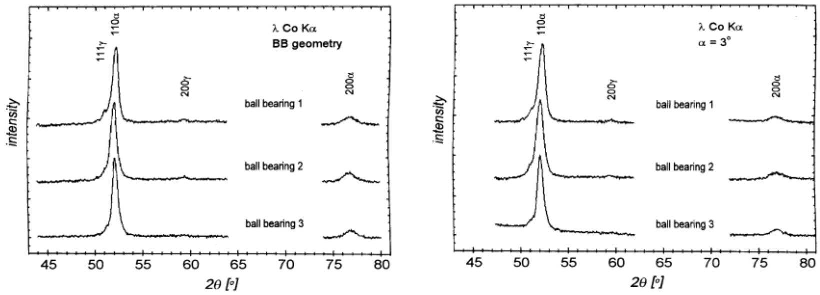

Fig. 2. Diffraction patterns of three sphere samples: BB geometry (left) and GID geometry for 3 deg. incident angles (right) [10].

Table 2. Quantitative phase analysis in the ball bearings of retained austenite (V_γ) and macroscopic residual stress (σ_I). Theoretical calculation for initial and final assumed content of the retained austenite as12 and 6 vol.%, respectively was curried out [10].

	Results and errors					
	Retained austenite, multi-peak method		Measured residual stresses [MPa]		Thickness (z) /incidence angle (α)	
Name	V_γ [%]	$\pm\Delta V_\gamma$ [%]	σ_I	$\pm\Delta\sigma$	z [μm]	α [deg]
kras1g3	*11,89*	*1,13*	*-791*	*70*	*3*	*3*
kras1g6	*12,79*	*1,06*	*-564*	*92*	*5,5*	*6*
kras1g9	*11,51*	*1,05*	*-357*	*32*	*7,5*	*9*
kras1g15	*5,57*	*0,90*	*-358*	*20*	*12*	*15*
kras2g3	5,62	0,65	-956	91	3	3
kras2g6	7,61	1,20	-906	26	5,5	6
kras2g9	11,06	1,06	-509	59	7,5	9
kras2g15	6,54	0,83	-648	22	12	15
kras3g3	*8,20*	*0,66*	*-811*	*107*	*3*	*3*
kras3Ag3	*8,56*	*0,85*	*-1144*	*79*	*5,5*	*6*
kras3g9	*11,33*	*1,07*	*-1108*	*98*	*7,5*	*9*
kras3g15	*10,12*	*1,11*	*-854*	*73*	*12*	*15*
Assumption/ calculation	12/6		-392		100	

Resulting differences in surface properties include volume fraction of retained austenite, residual stresses and surface hardness which increased by about 1-2 HRC units after burnishing.

Both Bragg-Brentano (BB) and grazing angle x-ray beam diffraction (GID) geometries were employed. Complete diffraction patterns were recorded with D8-Advances diffractometer (Fig.2). The data from diffraction patterns were used for quantitative phase analysis and residual stress evaluation (Tab.2).

4. Example – N27T2JMNb austenitic alloy (Skrzypek, Jeleńkowski 2006) [6]

This alloy is well characterized in term of strain induced phase transformation, microstructure after plastic deformation, thermal and mechanical stability. The surface layers of N27T2JMNb austenitic alloy were formed by surface mechanical treatments like grinding, polishing and burnishing.

Phase composition and residual stresses differ from sample to sample and versus depth under surface (Fig. 3, 4) [6]. The burnishing under 150 N of loading produced a large amount of strain martensite and microtwins in both i.e. in strain martensite and austenite (Fig. 4). **The presence of strain martensite and microtwins can be regard as a factors which increase diffusion during following nitriding.**

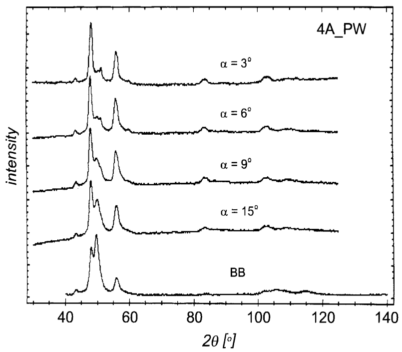

Fig.3. Example of qualitative phase analysis of nitrided sample after prior grounding, B-B and GID geometries, filtered CoK_{α} radiation. (different incidence angle (α) means different effective depth of penetration (z) i.e. for α=3 z=3.5, for α=6 z=7, for α=9 z=9-10, and for α=15 z=13-15μm, for BB geometry z=5-36μm [6].

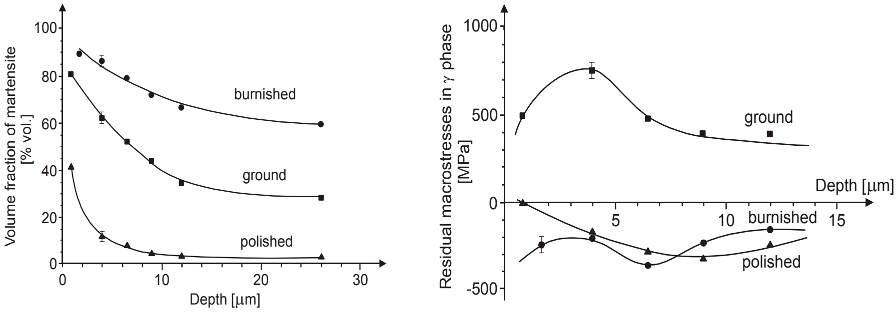

Fig. 4. Influence of surface preparation means on phase composition versus thickness of surface layer (depth under surface, left) and influence of surface preparation method on residual stresses distribution versus depth under surface (right) [6].

5. Complex oxide-carbide-nitride coatings (Dorzański, Skrzypek 2005) [4]

The sintered inserts made of the complex coatings: Al_2O_3+ZrO_2 , Al_2O_3+TiC on Si_3N_4 nitride coated by the PVD and CVD process were investigated. The inserts were multilayer coated by the PVD process – Cathodic Arc Evaporation (CAE) and by the CVD process [4]. Residual macrostresses were measured by GID-$\sin^2\psi$ method [1].

Table 3. Mechanical and functional properties of uncoated and coated ceramic tools are compared. Critical load describes adhesion beetwin substrate and coating, [4]

Substrate	Coating composition	Residual Stresses (g-$\sin^2\psi$ method), MPa	Hardness GPa	Critical load, Lc
Al_2O_3+ZrO_2 oxide ceramics	uncoated	-	18.5	-
	TiN+multiTiAlSiN+TiN	-170	40.9	76
	TiN+TiAlSiN+AlSiTiN	-141	21.0	78 (opt.)
Al_2O_3+TiC oxide ceramics	uncoated	-	19.7	-
	TiN+multiTiAlSiN+TiN	-216	40.3	71
	TiN+TiAlSiN+AlSiTiN	-120	30.7	77 (opt.)
Si_3N_4 nitride ceramics	uncoated	-	18.5	-
	TiC+TiN	616	19.8	67
	TiN+Al_2O_3	590	32.6	83
Si_3N_4 nitride ceramics (commercial inserts)	uncoated	-	18.5	-
	TiN+Al_2O_3+TiN	1008	24.4	48
	Al_2O_3+TiN	915	26.3	45

Finally it can be stated that both tension and compression residual stresses influence both micro-hardness, adhesion and resistance to abrasive wear of the examined coatings [4].

6. Eexamples of quality of cutting process (Ganev, Skrzypek, Sedlak [5] and (Ganev, Kraus) [9] which provide following experimental data on RS:

- plot of residual stress σ(x) vs width of lasser trace
- values of surface residual stresses σ(RS) and its gradients in the ferritic phase of the tool steel after electro discharge cutting using both graphite and copper electrodes
- average residual stresses σ(RS) in both the austenite and the ferrite of steel
- Residual stresses due to water jet cutting for different flow rate (water plus quartz sand): 560 g min^{-1} and 240 g min^{-1} flow rate caused RS in range from (–) 25 to (–) 336 MPa.

The provided data can be summarized: the level of RS after different method of cutting can be regarded as the quality factor of the cutting technology.

Conclusions

1. The surface mechanical treatments applied produced different surface layers in the ball bearings. These elastic-plastic strain induced phase transformation of retained austenite. The gradient like distribution of retained austenite versus depth under surface is non-linear.
2. Volume change in surface layers accompanied the phase transformation of retained austenite. Therefore macroscopic compressive residual stresses were created.
3. The measured macro-stresses were 2-3 times larger then that calculated theoretically when volume change due to phase transformation is taken into account.
4. The measured gradients of residual stresses distribution can increase error of classical $sin^2\psi$ method and it depends on geometry of measurnament and a range of ψ and θ angels.

Acknowledgements

Some research quoted here and this review paper was supported by Faculty of Metals Eng. and Industrial Computer Science, Department of Physical and Powder Metallurgy of AGH-UST in Krakow.

References

[1] Skrzypek S.J., New approach to residual macro-stresses measurement due to grazing angle X-ray diffraction geometry , *ROZPRAWY i MONOGRAFIE 108, Uczelniane Wyd. Nauk.-Dydaktyczne AGH*, Kraków 2002.

[2] Skrzypek S,J., Baczmański A., Ratuszek W., Kusior E., “New approach to stress analysis based on grazing-incidence X-ray diffraction” *Journal of Applied Crystallography* 34 (2001) pp.427-435.

[3] Cullity B.D. and Stock S.R., *Elements of X-ray Diffraction*, THIRD EDITION, Prentice Hall, Upper Saddle River, NJ07458, 2003.

[4] Dobrzański L.A., Skrzypek S.J., Pakuła D., Mikuła J.: Influence of the PVD and CVD technologies on the residual macro-stresses and functional properties of the gradient and multilayer coatings on the tool ceramics, *International Journal of Materials and Product Technology*, 2008.

[5] Ganev N., Skrzypek S.J., Sedlak P., Complex X-Ray Study of effect of mechanical surface treatment in shot-peened steels, *Inżynieria Materiałowa* nr 3 (2004) 576-582.

[6] S.J. Skrzypek, Jeleńkowski J., Borowski T., Wierzchoń T., Zakrzewski A., Non-destructive phase analysis and residual stresses measurement due to grazing angle X-ray diffraction geometry, EPDIC Praga Czech Republic 2004, *Z. fur Kristallographie*, 23 (2006) pp.375-380.

[7] Skrzypek S.J., Baczmański A., Progress in X-ray Diffraction of Residual Macro-stresses Determination Related to Surface Layer Gradients and Anisotropy, *Advances in X-Ray Analysis*, 44, (2001), pp.134-14.

[8] Evans H.E.: Stress effects in high temperature oxidation of metals. Inter. Mater. Reviews, 40, 1, 1995, pp.1–40.

[9] Ganev N., and Kraus I., Engineering Applications of X-Ray Stress Analysis, JCPDS-International Centre for Diffraction Data 2001,*Advances in X-ray Analysis*,Vol.44 pp.174-186.

[10] Skrzypek S.J., Goły M., Ratuszek W., Kowalski M., Non-Destructive Quantitative Phase and Residual Stress Analysis Versus Depth Using Grazing X-ray Diffraction *Solid State Phenomena* Vol. 130 (2007) pp.53-56.